

## Article

# Multicriteria Analytical Model for Mechanical Integrity Prognostics of Reactor Pressure Vessels Manufactured from Forged and Rolled Steels

Alvaro Rodríguez-Prieto <sup>1,2,\*</sup> , Manuel Callejas <sup>2</sup>, Ernesto Primera <sup>3,4</sup>, Guglielmo Lomonaco <sup>5,6</sup>   
and Ana María Camacho <sup>1</sup> 

- <sup>1</sup> Department of Manufacturing Engineering, Universidad Nacional de Educación a Distancia (UNED), 28040 Madrid, Spain; amcamacho@ind.uned.es
- <sup>2</sup> Department of Industrial Inspection and Technical Assistance, SGS Tecnos, 28042 Madrid, Spain; manuel.callejas@sgs.com
- <sup>3</sup> Department of Applied Statistics, University of Delaware, 531 South College Avenue, Newark, DE 19716, USA; eprimera@udel.edu
- <sup>4</sup> Machinery and Reliability Institute (MRI), 2149 Adair Ct, Mobile, AL 36695, USA
- <sup>5</sup> GeNERG, Dipartimento di Ingegneria Meccanica, TEC Division, Energetica, Gestionale e dei Trasporti (DIME), Università di Genova (UNIGE), Via all'Opera Pia, 15A, 16145 Genoa, Italy; guglielmo.lomonaco@unige.it
- <sup>6</sup> Istituto Nazionale di Fisica Nucleare (INFN), Sezione di Genova, Via Dodecaneso 33, 16146 Genoa, Italy
- \* Correspondence: alvaro.rodriguez@ind.uned.es; Tel.: +34-913-988-660



**Citation:** Rodríguez-Prieto, A.; Callejas, M.; Primera, E.; Lomonaco, G.; Camacho, A.M. Multicriteria Analytical Model for Mechanical Integrity Prognostics of Reactor Pressure Vessels Manufactured from Forged and Rolled Steels. *Mathematics* **2022**, *10*, 1779. <https://doi.org/10.3390/math10101779>

Academic Editors: Sambor Guze and Enrico Zio

Received: 18 April 2022

Accepted: 21 May 2022

Published: 23 May 2022

**Publisher's Note:** MDPI stays neutral with regard to jurisdictional claims in published maps and institutional affiliations.



**Copyright:** © 2022 by the authors. Licensee MDPI, Basel, Switzerland. This article is an open access article distributed under the terms and conditions of the Creative Commons Attribution (CC BY) license (<https://creativecommons.org/licenses/by/4.0/>).

**Abstract:** The aim of this work is to present a new analytical model to evaluate jointly the mechanical integrity and the fitness-for-service of nuclear reactor pressure-vessels steels. This new methodology integrates a robust and regulated irradiation embrittlement prediction model such as the ASTM E-900 with the ASME Fitness-for-Service code used widely in other demanding industries, such as oil and gas, to evaluate, among others, the risk of experiencing degradation mechanisms such as the brittle fracture (generated, in this case, due to the irradiation embrittlement). This multicriteria analytical model, which is based on a new formulation of the brittle fracture criterion, allows an adequate prediction of the irradiation effect on the fracture toughness of reactor pressure-vessel steels, letting us jointly evaluate the mechanical integrity and the fitness-for-service of the vessel by using standardized limit conditions. This allows making decisions during the design, manufacturing and in-service of reactor pressure vessels. The results obtained by the application of the methodology are coherent with several historical experimental works.

**Keywords:** prognosis; design-for-reliability; failure assessment diagram (FAD); pressure vessel; nuclear industry; irradiation embrittlement; analytical prediction model

**MSC:** 90B25

## 1. Introduction

The burning of fossil fuels, such as coal and oil, which account for two-thirds of all greenhouse gases [1], has dramatically increased the carbon dioxide content of the Earth's atmosphere over the last century [2]. Nuclear power, along with renewable options, is a clean alternative to decrease carbon dioxide emissions. The safe and long-term operation of nuclear reactors is one of the most discussed challenges in nuclear power engineering. The radiation-induced degradation of nuclear design materials limits the operational lifetime of all nuclear installations or at least decreases their safety margin [3]. Ferritic steels commonly used for the manufacture of reactor pressure vessels of light water reactors (LWR) exhibit in-service aging resulting in decreased ductility and toughness. In addition, diminished toughness has implications also for the reliability of this equipment under seismic loading conditions [4]. A reduction in the reliability of a component can cause

a series of undesirable consequences related to safety and competitiveness, as well as economic investments in maintenance and repair. In this way, the reliability of a component, and that of the equipment and/or system in which it is installed, is closely related to the number of failures that it will present in a given time interval. However, this reliability can be optimized by using advanced analysis models.

Data modeling is essential to mathematically characterize the trend in the behavior of the materials and components that define a system. On many occasions, the data obtained tend to show patterns (models or trends). Likewise, the use of IoT (Internet of Things) technologies makes it possible to have operation data in real time that can modify the “operating windows” considered, improving the adjustment of the model to the actual operating conditions. The developments in the fields of industrial Big Data technologies have made it possible to collect a lot of meaningful industrial processes and quality-based data that can be analyzed using contemporary statistical methods and machine learning techniques. Then, the extracted knowledge can be used for predictive maintenance or prognostic health management [5].

These strategies, therefore, make it possible to reduce the probability of failures (and their associated consequences), increase plant availability, minimize production losses and repair costs, as well as reduce the risk of fatal accidents. Decision making is the most critical and fundamental tool, which decision makers use to compare and rank different objects and alternatives based on a few particular criteria to make the best possible decision [6]. This is especially of interest in the materials selection processes for demanding applications such as nuclear power equipment. The nuclear reactor pressure vessel (RPV) comprises an enclosure of great thickness, typically between 200 and 300 mm, consisting of symmetrical elementary components of revolution connected together by welding end to end [7]. RPVs are made up of a cylindrical body and a hemispherical bottom and lid. The body and hemispheres are made up of rings that, in turn, are made up of curved and vertically welded sheets, although in some of the more recently manufactured vessels, there has been an attempt to avoid welding, for which complete forging pieces are manufactured [8]. The RPV is made up of special ferritic steels internally clad with stainless steel.

The steels used in the power production industry have been evolving continuously over the last few decades. The main advances have taken place in improving their mechanical behavior and their fracture toughness in order to avoid problems caused by brittle fractures when working in aggressive environments [9]. Because of the irradiation coming from the core, the beltline region of LWR pressure vessels experiences a slow deterioration of its mechanical properties, which is known as irradiation embrittlement. An accurate prediction of the severity of this phenomenon at each time during the operating life of the RPV is fundamental in order to prevent the vessel from experiencing stress states that may lead to a non-ductile propagation of a critical crack that may be present in the vessel walls, thus yielding vessel failure [10]. Tanguy et al. [11] performed different experiments to establish a comparison of fracture toughness with Charpy energy data for different levels of irradiation, showing that irradiation possibly causes a brittle fracture. During long-term operation, the fast neutron fluence causes the ferritic steel of RPV to be susceptible to brittle fracture, especially in the beltline region corresponding to the reactor core. The embrittled vessel shell may fracture due to a preexisting fabrication flaw and leads to a through-wall crack [12]. Nevertheless, the use of Charpy data from experimental testing is a time-consuming strategy to estimate ductile-to-brittle transition temperature. Thus, the selection of RPV steel based on the suitability against irradiation embrittlement can be addressed not only by performing trial-error testing [13] but also by performing analysis combining consolidated prediction models with other standardized methodologies.

Ductile-to-brittle transition refers to an observable change in fracture mode with decreasing temperature—from slow ductile crack growth to rapid cleavage. It is exhibited by body-centered cubic metals and presents a challenge for the integrity assessment of structural components made of such metals [14]. Neutron irradiation embrittlement of RPV steels causes the most severe damage during the operation of nuclear power plants [15];

therefore, it is considered crucial to perform a prognosis, in the design phase, of the mechanical integrity conditioned by the irradiation embrittlement. It is, in general, essential to investigate correlations between the microstructure and properties of materials [16]. Over recent decades, irradiation hardening and embrittlement have been widely observed in nuclear structural materials with different crystalline structures [15,17–20], e.g., face-centered cubic (FCC) [21–24], body-centered cubic (BCC) [25–27] and hexagonal close-packed (HCP) [28–30] materials [31]. Crystals present both translational and orientational properties of symmetry, which govern their physical properties [32].

Odette et al. [33] concluded that, in ferritic steels typically used in the manufacture of RPV, pernicious copper-rich precipitates are generated during irradiation that are responsible for irradiation embrittlement in RPV materials. The core structure for a small copper-rich precipitate, composed of three rows along with the dislocation core, changes dramatically from symmetric to nonsymmetric (degenerate) during irradiation [34]. In addition, another intriguing phenomenon under radiation is the self-organization of defects, such as the void superlattices, which have been observed in a list of BCC and FCC metals and alloys when the irradiation conditions fall into certain windows defined by temperature and dose rate. Thus, symmetry breaking is induced by anisotropic vacancy diffusion [35].

Structural components located near nuclear fuel assemblies in LWRs are exposed to intense radiation fields. Neutron irradiation causes significant changes in material properties and, in some cases, results in the degradation of structural integrity [36]. Neutron irradiation affects the material properties and hence the structural integrity of reactor pressure vessels in nuclear power plants. Mitigation of irradiation damage is one of the major issues within nuclear plant life management [37].

The ASME code [38] states that for both non-irradiated and irradiated vessel materials, the variation in fracture toughness with temperature is indexed through the transition temperature called  $RT_{DBT}$  (reference temperature). To determine experimentally the value of the  $\Delta RT_{DBT}$  (ductile-to-brittle transition temperature shift) and, therefore, the fracture toughness ( $K_{IC}$ ) of the irradiated material, monitoring capsules are included in the vessel between the core and the wall. These capsules contain specimens of the vessel material, both welds and thermally affected zone and base material. The surveillance capsules are periodically removed in order to test the specimens, which allows us to know in advance the state of the material that makes up the vessel. The capsules include tensile, Charpy impact and fracture toughness specimens, as well as the instrumentation necessary to monitor neutron fluence and temperature [8]. Traditional material research relies on a considerable amount of experimental trial designs, which are time-consuming and costly [39]. There are several consolidated prediction models to estimate the  $\Delta RT_{DBT}$  in irradiated RPV steels; these are mainly the NUREG/CR-6551 [40] and ASTM E-900 [41]. Therefore, it could be possible to obtain the  $K_{IC}$  from the calculated  $\Delta RT_{DBT}$ , reformulating the customary  $K_{IC}$  determination schemes.

Symmetry is usually integrated into different considerations for calculation. The applied loads are considered symmetrical, and the crack is initiated and propagated symmetrically from this position [42]. Symmetry is also found inside a cross-section of a nuclear power reactor core [43]; therefore, the neutron incidence can also be considered symmetric. For a long time, cracked structures have triggered various researchers to develop a structural integrity approach and design models to address the fracture problems [44]. The consequences of a failure can have a negative impact on the structure of machines, employees and the environment [45]. In addition, it is crucial to study damaged materials (for example, materials with cracks and with unduly chemical composition restrictions) to assess the fitness-for-service along with the mechanical integrity. The use of analytical prediction methods allows saving time and cost related to the performance of experimental tests with the aim of making a decision on the suitable selected material that prevents future failures.

The aim of this work is to present a new analytical model to evaluate jointly the mechanical integrity and the fitness-for-service of nuclear reactor pressure-vessel steels, considering a robust and regulated irradiation embrittlement prediction model, ASTM E-900 [41], and the fitness-for-service calculations used widely in other demanding industries such as oil and gas. This methodology involves the analysis and correlation between multiple chemical and mechanical requirements to evaluate, among others, the risk of experiencing degradation mechanisms such as brittle fracture (promoted, in this case, by the irradiation embrittlement). The components analyzed in this study are pressurized with the following mean operating conditions:  $1.80 \times 10^6$  Pa of pressure (P), a range of neutron fluence of  $\phi = 1\text{--}5 \times 10^{19}$  n/cm<sup>2</sup> and an irradiation temperature (T) up to 300 °C.

Therefore, the analytical model, which is based on a new formulation of the brittle fracture criterion, allows an adequate prediction of the irradiation effect on the fracture toughness of reactor pressure vessel steels, letting us jointly evaluate the mechanical integrity and the fitness-for-service of the vessel by a novel methodology; that, finally, includes very practical elements such as failure assessment diagrams (FAD) and risk matrixes, very useful for the industry.

## 2. Methodology

The analytical methodology (Figure 1) is divided into four steps: a  $\Delta RT_{DBT}$  estimation based on the U.S. Nuclear Regulatory Commission (NRC) ASTM E-900 prediction model (Step 1), followed by an adaptation of the ASME Fitness-For-Service (FFS) code to obtain the fracture toughness ( $K_{IC}$ ) considering standardized limit conditions (Step 2) and the construction of a FAD and a risk matrix of integrity loss (Step 3). Finally, a validation of limit conditions and results based on the conclusions from experimental works is performed (Stage 4).

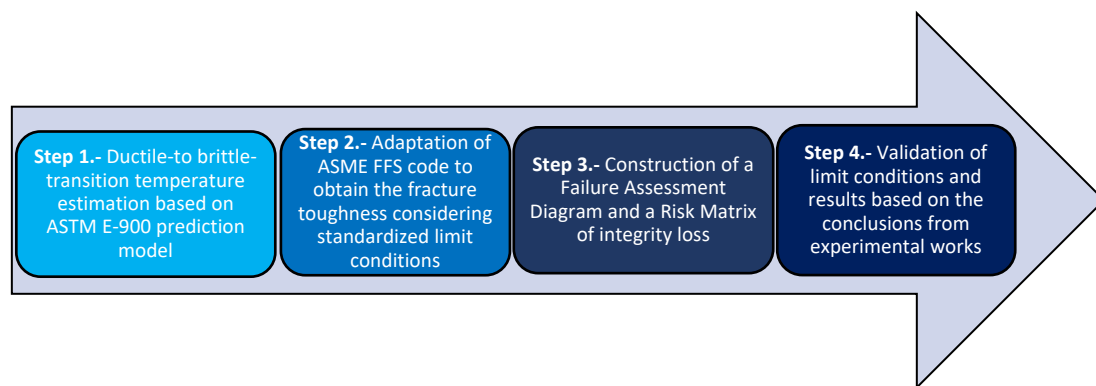


**Figure 1.** Methodology to perform mechanical integrity prognostics.

### 2.1. Step 1—Ductile-to Brittle-Transition Temperature Estimation Based on ASTM E-900 Prediction Model

The reactor pressure vessel (RPV) in LWR represents a fundamental line of defense against a release of radiation in case of an accident [46]. Thus, regulations that govern the operation of commercial nuclear power plants require conservative margins of fracture toughness, both during normal operation and under accident scenarios [47]. The correct interpretation of the significance of defects, in terms of the probability of in-service failure, requires considerable skill; this is because many of the primary properties (such as embrittlement), which ultimately influence service performance, cannot be monitored directly so that one has to find some relationship between these properties and those structural defects which can be monitored either during fabrication or during service [48]. Materials of nuclear reactor pressure vessels exposed to neutron radiation that is generated by nuclear fission reactions experience appreciable damage at even very low doses of radiation, producing embrittlement and a shift of the ductile-to-brittle transition temperature ( $\Delta RT_{DBT}$ ). Nanoscale microstructures induced by irradiation obstruct the migration of

dislocations, and this interaction prevents plastic deformation and induces steel embrittlement [27]. Neutron irradiation degrades the mechanical properties of RPV steels, and the extent of the degradation is determined by the type and structure of the steel and other factors such as neutron fluence, irradiation temperature, neutron fluence and chemical composition [8,26,27]. At the reactor operating temperature, the vessel material exhibits a ductile behavior. However, the constant bombardment of neutrons on the walls of the vessel produces a decrease in its mechanical properties, losing its ductility and being brittle at increasingly higher temperatures.

The degree of embrittlement depends on the fuel distribution, the neutron spectrum to which the vessel wall is subjected and the operating temperature. Therefore, the experts present a basic safety criterion, ensuring sufficient toughness of the steel of the vessel throughout its useful life. The quantification of this effect is carried out by evaluating the displacement experienced by the  $\Delta RT_{DBT}$ . Often, displacements of up to 200 °C have been recorded [40,49]. The method is developed around the concept of reference temperature ( $RT_{DBT}$ ), below which brittle fracture occurs even in the presence of small notches and from which the phenomenon of the ductile-brittle transition develops [50]. Figure 2 exhibits a scheme that represents the displacement of  $K_{IC}$  and  $\Delta RT_{DBT}$  due to neutron irradiation.  $K_{IC}$  after irradiation ( $RT_{DBT-I}$ ) is diminished with respect to the previous value before irradiation (typically between a neutron fluence,  $\phi$ , between 1 and  $5 \times 10^{19}$  n/cm<sup>2</sup>).

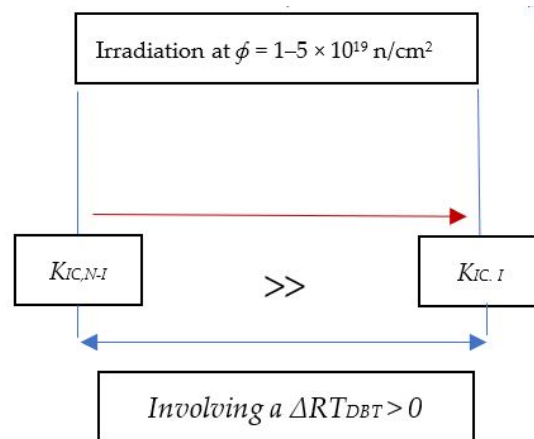


Figure 2. Irradiation effect on  $K_{IC}$  and  $\Delta RT_{DBT}$ .

RPV steels are exposed to neutron radiation, and their ductile-to-brittle transition temperature before irradiation ( $RT_{DBT-NI}$ ) experienced a shift ( $\Delta RT_{DBT}$ ) changing, therefore, towards a higher transition temperature ( $RT_{DBT-I}$ ), as Equation (1) provides.

$$RT_{DBT-I} = RT_{DBT-NI} + \Delta RT_{DBT} \tag{1}$$

However, by using prediction models such as ASTM E900-02, it is possible to accurately estimate the  $\Delta RT_{DBT}$  allowing to estimate further the fracture toughness after irradiation ( $K_{IC-I}$ ) by using the analytical scheme given in ASME code [51] to be used finally in the calculation scheme of ASME FFS-1 [52].

ASTM E900-02 prediction model

ASTM E900-02 [41] provides improvements with respect the historical R.G. 1.99 Rev.2 prediction model [53]. Thus, Equation (2) shows the main two terms that grouped several calculation parameters.

$$\Delta RT_{DBT} = SMD + CRP \tag{2}$$

$SMD$  term (Equation (3)) is related to stable matrix defects, which are defined as complex vacancy solute clusters and nanovoids, which do not fully dissolve over an extended period of time [54]. The  $CRP$  term (Equation (4)) is associated with copper-

rich precipitates that causes hardening. These three terms could be calculated by using Equations (3)–(6).

$$SMD = A \exp \left[ \frac{C_{Tc}}{T_c + 460} \right] [1 + C_P P](\varphi t)^\alpha \tag{3}$$

$$CRP = B [1 + C_{Ni} Ni^\eta] F(Cu) G(\varphi t) \tag{4}$$

CRP contribution is calculated by obtaining the  $F(Cu)$  (Equation (5)) and the  $G(\varphi t)$  (Equation (6)) parameters.

$$F(Cu) = \{0, Cu \leq Cu_{th}; (Cu - Cu_{th}), Cu > Cu_{th}\} \tag{5}$$

$$G(\varphi t) = 1/2 + 1/2 \tanh \left\{ \frac{[\log(\varphi t + C_t t_f) - \mu]}{\sigma} \right\} \tag{6}$$

The used calculation parameters are shown in Table 1.

**Table 1.** Parameters used in the SMD and CRP calculation according to ASTM E900-02 model [40,55–57].

SMD Term		CRP Term	
Description	Value Used	Description	Value Used
$A_{forging}, A_{plates}$	$6.70 \times 10^{18}$	$B_{forging}$	128
$C_{Tc}$	$2.07 \times 10^4$	$B_{plates}$ Note 4	208 (156)
$T_c$ Note 1 (°F)	572	$C_{Ni}$	2.106
$C_P$	0	$Ni$ (wt%)	0–1.2
$P$ Note 2 (wt%)	0.02	$\eta$	1.173
$\varphi t$ Note 3 (n/cm <sup>2</sup> )	$3 \times 10^{19}$	$\kappa$	0.577
$\alpha$	0.5076	$Cu_{th}$	0.072
		$Cu$ (wt%)	0–0.4
		$\Phi t$ (n/cm <sup>2</sup> )	$3 \times 10^{19}$
		$C_t$	0
		$\mu$	18.24
		$t_f$ Note 5 (h)	360,000

Note 1: Selected operating temperature  
 Note 2: Limit proposed by Amayev et al. [56] to limit pernicious effects on mechanical behavior  
 Note 3: Neutron fluence rate  
 Note 4: 156 for rolled materials without CE mark  
 Note 5: Considered 40 years of design

The fracture toughness of a material is conventionally assessed in terms of the critical value of some crack tip field characterizing parameters at the initiation of unstable crack growth [58].

When fracture toughness data are not available, an estimation procedure based on the  $RT_{DBT}$  can provide fracture toughness for ferritic steels. The Equation (7) for the fracture toughness mode 1 ( $K_{IC}$ ) curve is given by [59], where  $T$  is the operating temperature:

$$K_{IC} = 36.5 + 22.783 \exp [0.036(T - RT_{DBT})] \text{ (MPa } \sqrt{\text{m}}, \text{ } ^\circ\text{C)} \tag{7}$$

The ASME B&PV code [59] describes the use of mode 1—opening mode (tensile stress normal to the plane of the crack) that is used in the methodology used in this research work.

### 2.2. Step 2—Adaptation of ASME FFS Code to Obtain the Fracture Toughness Considering Standardized Limit Conditions

API 579-1/ASME FFS-1, Fitness-For-Service [51] is a recognized standard developed by the American Society of Mechanical Engineers (ASME) and by the American Petroleum Institute (API) that describes several fitness-for-service (FFS) assessment methodologies for pressurized equipment used mainly in the oil and gas, as well as chemical and petrochemical industries. This code contains several sections related to the assessment procedures for calculating the consequences on the installation safety due to damage mechanisms such as a brittle fracture or different types of corrosion, among many others. It is well known that the brittle crack propagation is governed by the stress intensity factor at the crack edges. When it is exceeded a critical value of fracture toughness ( $K_{IC}$ ), referred as plain strain fracture toughness, the propagation occurs.  $K_{IC}$  depends on the type of crack and, in

particular, on the actual toughness of the material, i.e., the toughness calculated accounting for the irradiation effect [10].

The toughness is the resistance of a material to brittle fracture when a crack is present.

The  $K_{IC}$  parameter is a measure of the material’s resistance to brittle fracture in plane strain and is usually known as the fracture toughness in plane strain. The rapid crack extension is predicted to occur when  $K$  reaches  $K_{IC}$ , with  $K_{IC}$  being a unique material property for a given material condition, temperature, and loading rate. Stress intensity factor based on primary stresses ( $K_I^P$ ) calculated in surface and deepest part of a crack of 1.5 mm (maximum allowable dimension—before considering this a relevant indication—according to ASME B&PV VIII [60]), considering that secondary stresses and residual stresses are null. The stress intensity factor ( $K_I$ ) is calculated [51] as follows (Equation (8)):

$$K_I = \sigma_1 G_1 \left(\frac{a}{t}\right)^2 \sqrt{\frac{\pi \cdot a}{Q}} \tag{8}$$

where

$$Q = 1 + 1.464 \left(\frac{a}{c}\right)^{1.65} \tag{9}$$

$a/c = 1, a = 1.6$  mm and  $a/t = 0.01$  if  $t = 245$  mm (typical mean thickness of a PWR-RPV).  
 $G_1 = 0.1870117$  for zero order ( $A_0$ ) for  $a/c = 1, t/R_i = 0.11$  if  $R_i = 2200$  mm (typical mean radius of a PWR-RPV).

$\sigma_1 = 1.80 \times 10^6$  Pa.

The toughness ratio is calculated by using Equation (10):

$$K_r = \frac{K_I^P + \phi K_I^{SR}}{K_{IC}} = \frac{K_I^P}{K_{IC}} \tag{10}$$

if  $\phi K_I^{SR} = 0$  considering null the plasticity interaction factor

From fracture mechanics testing of RPV steels, a  $K_{IR}$  curve was established as a lower bound curve that has to be used in the design phase [61].

### 3. Results

#### 3.1. Step 3—Construction of a Failure Assessment Diagram (FAD) and a Risk Matrix of Integrity Loss

To evaluate the suitability for service based on the response against the irradiation embrittlement, an assessment is performed by defining first the brittle collapse scenario (a) to represent a failure assessment diagram—FAD (b) and, finally, to construct a risk matrix (c).

This type of diagram is very useful for performing design-for-reliability tasks that reduce the necessity of trial-and-error tests and allow to improve the safety of the design.

##### (a) Brittle collapse of cracked section

For brittle failure situations in cracked components, in which linear-elastic behavior is dominant, fracture mechanics establishes that fracture occurs when the applied stress intensity factor ( $K_I$ ) is equal to the material fracture toughness ( $K_{IC}$ ) [62]. The crack ignition occurs if  $K_I \geq K_{IC}$ .  $K_{IC}$  is calculated as Equation (7) indicated, and ratio  $K_r$  can be defined (Equation (11)).

$$K_r = \frac{K_I}{K_{IC}} \tag{11}$$

$K_I$  = stress concentration factor applied under normal conditions on the crack.

$K_{IC}$  = fracture toughness based on crack initiation determined at crack end temperature.

Then, if  $K_r < 1 \rightarrow$  safety zone and brittle fracture occurs if  $K_r \geq 1$ .

For fracture assessments, the plane of the flaw hall is assumed to be normal to the maximum principal tensile stress [52].

##### (b) Construction of the FAD

Once obtained  $K_r$ ,  $L_r$  is calculated to be a similar scheme to BS 7910 [63]. However,  $L_r$  cutoff value  $L_{r(max)}^P$  is, in this case, given by the ratio, showing a characteristic value for every material analyzed (Equation (12)):

$$L_{r(max)}^P = \frac{\sigma_{TS} - \sigma_{YS}}{\sigma_{YS}} \tag{12}$$

where

$\sigma_{YS}$ : Yield strength.

$\sigma_{TS}$ : Ultimate tensile strength.

The maximum  $L_r$  threshold value,  $L_{r(max)}^P$ , should also be applied to the calculated FAD curve to determine the plastic collapse limit [52]. The fracture assessment of much-pressurized equipment is conducted using a FAD assessment similar to the specified in BS 7910 [63–66]. Figure 3 provides a failure assessment diagram focused on the brittle fracture of reactor pressure-vessel steels.

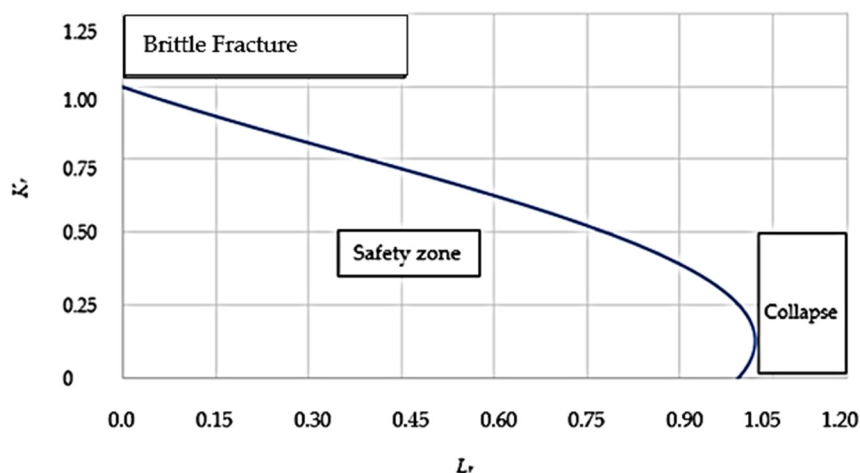


Figure 3. Failure assessment diagram.

As observed in Figure 3, the safety zone is constrained under  $K_r = 1$  and  $L_r = 1$ . The material, therefore, would be susceptible to experiencing brittle fracture when  $K_r > 1$ , and it can suffer collapse if  $L_r$  is greater than 1. The standardized requirements for chemical composition of materials [8] analyzed are shown in Table 2. They are necessary to obtain the potential  $\Delta RT_{DBT}$  based on materials’ chemical requirements and the irradiation and temperature conditions using the calculation parameters indicated in Table 1.

Table 2. Chemical limits used in the analysis.

RPV Material	Chemical Requirements (Maximum wt%)	
	Cu	Ni
ASTM A 212 B (rolled)	N.S.	N.S.
ASTM A 302 B (rolled)	N.S.	N.S.
ASTM A 543 B (rolled)	N.S.	4.00
A 336 (rolled)	N.S.	0.50
ASTM A 533 Grade B Cl.1 (rolled)	0.12	0.73
JIS G-3120 SQV2 A (rolled)	N.S.	0.70
ASTM A 508 Grade 2 (forging)	0.20	1.00
ASTM A 508 Grade N (forging)	0.25	3.90
DIN 22NiMoCr37 (forging)	0.11	1.00
ASTM A 508 Gr. 3 (forging)	0.20	1.00
DIN 20MnMoNi55 (forging)	0.12	0.85
RCC 16 MND5 (forging)	0.20	0.80
JIS G 3204 SFVQ1A (forging)	N.S.	1.00

Table 2. Cont.

RPV Material	Chemical Requirements (Maximum wt%)	
	Cu	Ni
ASTM A 336 Grade F22V (forging)	0.20	0.25
ASTM A 336 Grade F91	N.S.	1.50
WWER 15Kh2MF (forging)	0.30	0.40
WWER 15Kh2MFA (forging)	0.30	0.40
WWER 15Kh2NMFA (forging)	0.30	0.40
WWER 15Kh2NMFAA (forging)	0.08	0.40

Note 1: NS—not specified.

Thus, Figure 4 provides the estimated  $K_r$  (calculated from Equations (8)–(11)) for several materials used in the manufacturing of reactor pressure vessels, covering materials used in different generations of reactors.

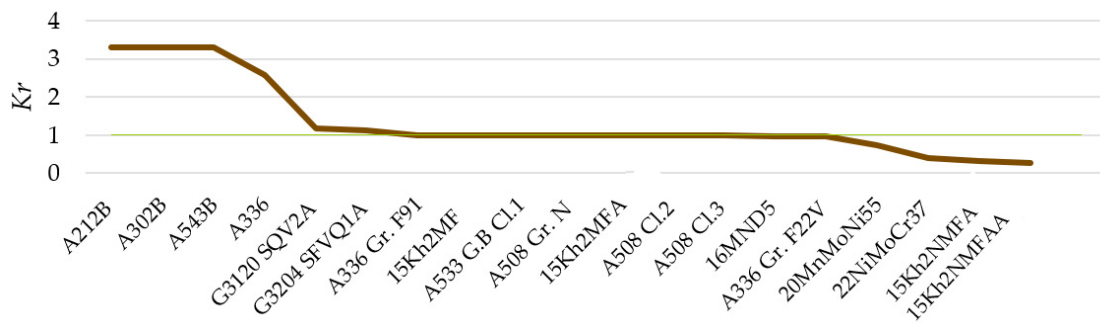


Figure 4.  $K_r$  for the materials analyzed.

As Figure 4 demonstrates, the materials with less susceptibility to brittle fracture are materials developed for the second generation of reactors and so on, i.e., the A336 Gr. F91, 15Kh2MFA, A533 Gr. B Cl.1, A508 Gr. N, 15Kh2MFA, A508 Cl.2, A508 Cl.3, 16MND5, A336 Gr. F22V, 20MnMoNi55, 22NiMoCr37, 15Kh2MFAA and 15Kh2NMFAA.

Thus, 15kh2NMFAA, 15kh2MFAA, 22NiMoCr37 and 20MnMoNi55 provide the lower  $K_r$ . On the other hand, materials developed for the first generations (A212B, A302B, A543B and A336) provide greater values of  $K_r$ . G3120 SQV2A and G3204 SFVQ1A are just in the limit ( $K_r = 1$ ).

Figure 5 exhibits  $L_r$  for each material analyzed.

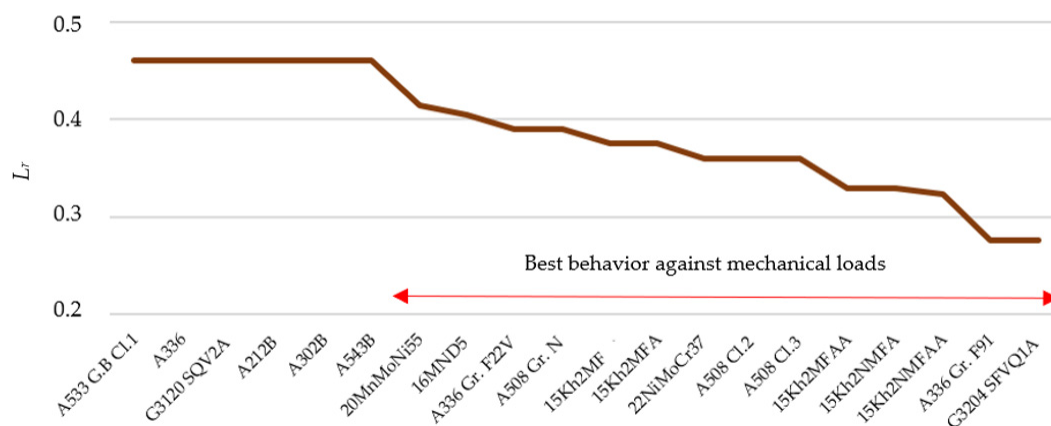


Figure 5.  $L_r$  for every analyzed material.

When  $L_r$  is lower, the response to mechanical loads is more efficient (from an approach focused on the mechanical integrity of material), generating less permanent deformation (the ratio  $\sigma_{TS}/\sigma_{YS}$  is lower). On the other hand, if the  $K_r$  is higher, the susceptibility to

brittle fracture is greater. As Figure 5 provides, the mechanical response of plates (rolled materials) is, in general, poorer than forging materials.

(c) Construction of Risk Matrix

To construct the risk matrix, risk of integrity loss (*RIL*) is defined as (Equation (13)):

$$RIL = K_r \cdot L_r \tag{13}$$

Figure 6 provides the *RIL* matrix for the materials analyzed that serves as a decision matrix for the most suitable material to prevent potential failures. Thus, the minimum risk is provided by the 15Kh2NMFAA, 15Kh2MFAA, 22NiMoCr37, 20MnMoNi55, A336 Gr. F22V, A508 Cl.2, A508 Cl.3, 16MND5, A336 Gr. F91 and A508 Gr. N.

Therefore, the selection criteria related to reducing the brittle fracture susceptibility are minimized the *RIL* value. Subsequently, a multicriteria matrix representation is a visual and easy way to show the *RIL* of best options (according to obtained  $K_r$  and  $L_r$  values) analyzed materials, allowing to extract conclusions such as the materials with lower RTBF (very low risk) correspond to the most consolidated standards (15Kh2NMFAA, 15Kh2MFAA, 22NiMoCr37 and 20MnMoNi55) followed by other consolidated and new standards (A508 Cl.2, A508 Cl.3, 16MND5 and A336 Gr. F22V).

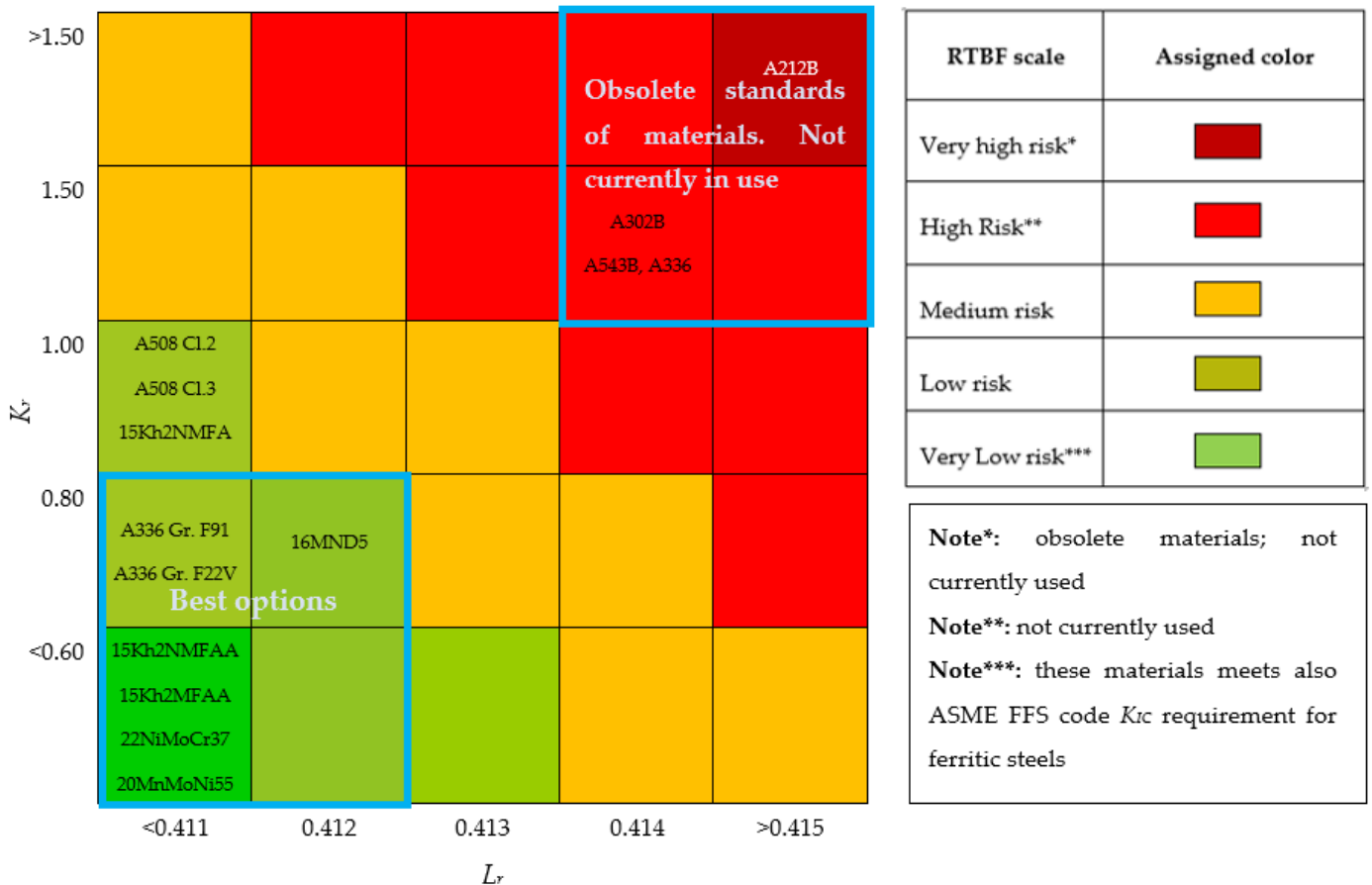


Figure 6. Risk matrix according to *RIL*.

As Figure 6 exhibits, more used materials specifications used in the modern designs of reactors provide a low *RIL*. In addition, the specifications 15Kh2MFA, 15Kh2NMFA, 20MnMoNi55 and 22NiMoCr37 meet the  $K_{IC}$  requirement established by ASME FFS for ferritic steels. These materials have as a characteristic a very stringent control of impurities, so the mechanical integrity prediction by the analytical model presented in this work is very sensitive to impurities restrictions.

3.2. Step 4—Validation of Limit Conditions and Results Based on the Conclusions from Experimental Works

Determination of  $K_{IC}$  on the upper shelf would be impracticable since it would require big specimens. ASME FFS-1 [52] provides, therefore, a threshold of  $K_{IC}$  equal to  $220 \text{ MPa} \cdot \sqrt{\text{m}}$ , valid for ferritic steels, aligned with the requirement for the ASME B&PV code [38] reference curve. On the other hand, from  $150 \text{ }^\circ\text{C}$ , the irradiation embrittlement is less severe due to annealing effects [67], as demonstrated by experimental works [55,68,69]. Figure 7 shows the predicted  $K_{IC}$  for every studied material.

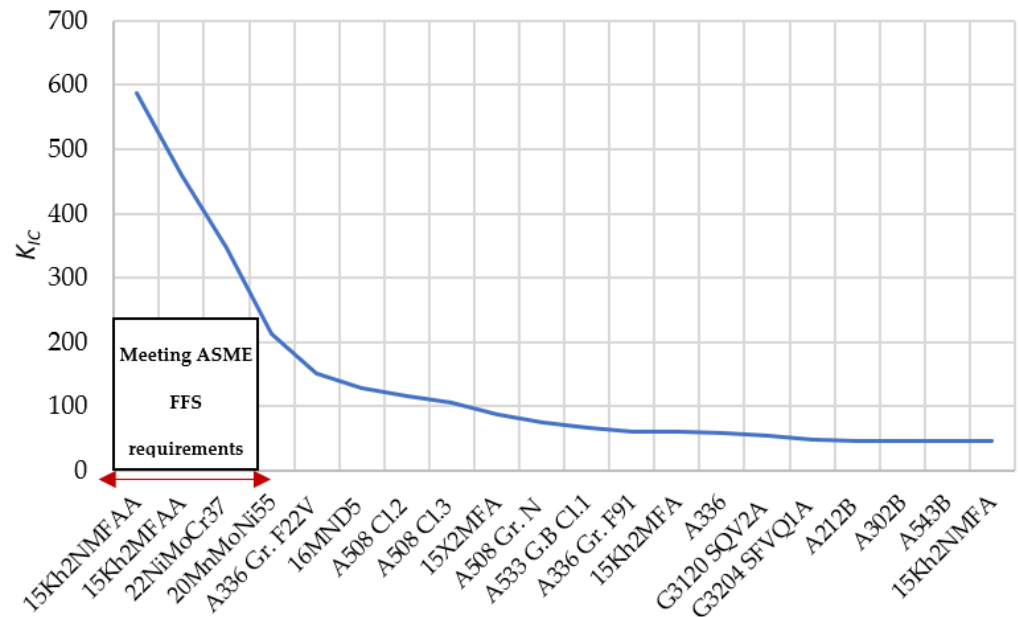


Figure 7.  $K_{IC}$  for the materials analyzed.

Analogously, the application of the  $K_{IC, min}$  (minimum required value of fracture toughness) constraint for ferritic steels provided by ASME FFS-1 [52] shows the same best options: 15kh2NMF AA and 15kh2MF AA (both with very stringent control of impurities) as well as the 22NiMoCr37 and 20MnMoNi55. All of these specifications are highlighted due to their very stringent mechanical and chemical requirements. Figure 8 provides, for the material 15kh2NMF AA, the  $K_{IC}$  variation versus in-service temperature compared with the minimum required  $K_{IC}$  according to ASME FFS. Thus, from  $T = 85.5 \text{ }^\circ\text{C}$ ,  $K_{IC, mean}$  is greater than  $220 \text{ MPa} \cdot \sqrt{\text{m}}$  since it could be considered as a minimum temperature to ensure that the minimum value of  $K_{IC}$  is always reached.

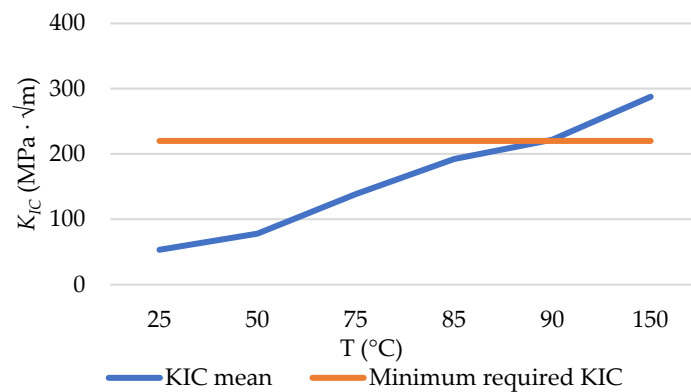


Figure 8.  $K_{IC}$  variation versus temperature compared with the minimum required  $K_{IC}$  according to ASME FFS.

Figure 9 provides  $K_{IC}$  versus typical values of Cu wt% and Ni wt% in the ferritic steels used in the manufacture of reactor pressure vessels. This figure also indicates the maximum Cu and Ni wt.% contents to meet the  $K_{IC}$  requirements established by the ASME FFS code.

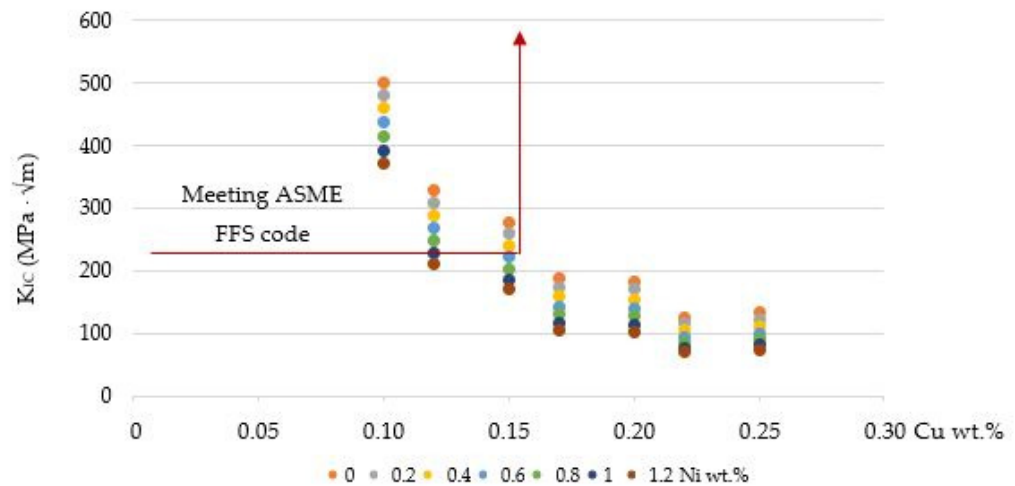


Figure 9.  $K_{IC}$  versus Cu wt% and Ni wt%.

For most unirradiated mild steels, the  $\Delta RT_{DBT}$  is between  $-50$  °C and  $20$  °C. The process of irradiation hardening, through the formation of clusters of interstitial or vacancy defects, increases the friction stress of these steels and thereby raises the transition temperature [70].

Using the maximum  $\Delta RT_{DBT}$  specified by KTA 3203 to avoid additional safety calculations [71], i.e.,  $40$  °C, and assuming a considered maximum  $RT_{DBT,N-I} = 50$  °C according to Fisher et al. [68], the maximum  $RT_{DBT,I}$  would be equal to  $90$  °C. The result obtained (maximum  $RT_{DBT,I} = 85.5$  °C to meeting the ASME FFS  $K_{IC}$  requirements, i.e., a minimum  $K_{IC}$  equal to  $220$   $\text{MPa} \cdot \sqrt{\text{m}}$ ) by using this novel methodology is coherent with the maximum  $RT_{DBT,I}$  according to experimental works and the limits (based on a large operational experience) provided by KTA 3203 [71].

To keep  $K_{IC} > 220$   $\text{MPa} \cdot \sqrt{\text{m}}$ , Cu wt% is 0.15 and Ni wt% 0.60 that is more stringent than predictions based on other models:  $\text{Cu} \leq 0.16, \forall 0.4 < \text{Ni} \leq 0.6 \forall \text{P}$  according to R.G. 1.99 Rev.2 [53];  $\text{Cu} \leq 0.15, \forall \text{Ni} < 0.6$  and  $\text{P} < 0.02$  according to NUREG CR 6551 [40] and  $\text{Cu} \leq 0.15, \forall 0.2 \leq \text{Ni} < 1.2$  and  $\text{P} < 0.02$  according to ASTM E900-02 [41]. In addition, the results obtained verify the observation performed by Fisher et al. in which  $K_{IC}$  varies from about  $35$   $\text{MPa} \cdot \sqrt{\text{m}}$  (at  $T = \Delta RT_{DBT} - 50$  °C) to about  $200$   $\text{MPa} \cdot \sqrt{\text{m}}$  (at  $T = \Delta RT_{DBT} + 50$  °C) [10]. Thus, a  $\Delta RT_{DBT} > 14.5$  °C (according to the calculation provided by Equation (1)) implies a  $K_{IC}$  similar ( $220$   $\text{MPa} \cdot \sqrt{\text{m}}$ ) to that one required by ASME FFS ( $220$   $\text{MPa} \cdot \sqrt{\text{m}}$ ). Therefore, it would be recommended that the brittle fracture should be specially monitored under  $150$  °C. This agrees with the conclusions of Pachur [67] that showed as an irradiation temperature of  $150$  °C produces the greatest fragility of the material, being this less for a higher temperature. This is due to the fact that an increase in the irradiation temperature favors the repair of defects produced by neutron bombardment through a process of annealing the material [67].

By applying this methodology, a  $220$   $\text{MPa} \cdot \sqrt{\text{m}}$  is only obtained with a Cu wt% restriction of 0.15% and a Ni wt.% restriction of 0.60%. Therefore, these restrictions are interesting to be considered in preliminary materials selection tasks performed in the equipment design phase [72]. Since the  $K_{IC}$  is a parameter that is increased with the temperature, the requirements of Cu wt.% and Ni wt.% content are more stringent for a lower temperature, as Figure 10 shows.

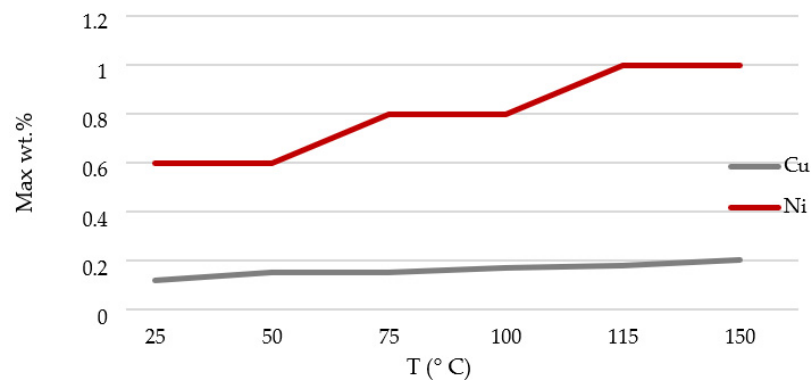


**Figure 10.** Maximum Cu wt.% and Ni wt.% versus operation temperature to ensure a  $K_{IC}$  lower than  $220 \text{ MPa} \cdot \sqrt{\text{m}}$ .

#### 4. Conclusions

In this work, a novel analytical methodology to predict the in-service mechanical integrity of rolled and forging steels—used in the manufacture of RPV—has been proposed. The methodology connects two robust models such as ASTM E900 and ASME FFS code to predict the  $K_{IC}$  using standardized requirements. Thus, the suitability of several materials has been estimated. In addition, the results from the methodology have been validated by comparing with experimental results from well-established and recognized historical research works.

In the new methodology, several new elements have been incorporated, such as the use of the fitness-for-service calculations concept and the construction of a risk matrix, allowing a multiperspective approach that helps find the suitable solution to ease the arduous material selection task in a demanding industry such as the nuclear one. The analytical model, which is based on a new formulation of the brittle fracture criterion, has allowed an adequate prediction of the irradiation effect on the fracture toughness of reactor pressure vessel steels, letting us jointly evaluate the mechanical integrity and the fitness-for-service of the vessel by a novel methodology. The major conclusions from this work can be summarized as follows:

- The matrix representation shows the *RIL* of the best options of analyzed materials (according to obtained  $K_r$  and  $L_r$  values), allowing to extract conclusions such as the materials with lower *RIL* (very low risk) correspond to the most consolidated standards (15Kh2NMFAA, 15Kh2MFAA, 22NiMoCr37 and 20MnMoNi55) followed by other consolidated and new standards (A508 Cl.2, A508 Cl.3, 16MND5 and A336 Gr. F22V). These forging materials are consolidated grades used in the PWR 3-4 generation and, therefore, are currently still in operation. In addition, other historical forging grades such as 16MND5 show very safe conditions.
- Obsolete materials specifications (A212B, A302B, A543B and A336) provide the worst mechanical integrity, corresponding these materials to rolled materials.
- It has been concluded that, according to the methodology, to keep  $K_{IC} > 220 \text{ MPa} \cdot \sqrt{\text{m}}$  as required by ASME FFS code [52], Cu wt% should be lower than 0.15 and Ni wt% lower than 0.60; these limits are more stringent than predictions based on other models:  $\text{Cu} \leq 0.16, \forall 0.4 < \text{Ni} \leq 0.6 \forall P$  according to R.G. 1.99 Rev.2 [53];  $\text{Cu} \leq 0.15, \forall \text{Ni} < 0.6$  and  $P < 0.02$  according to NUREG CR 6551 [40] and  $\text{Cu} \leq 0.15, \forall 0.2 \leq \text{Ni} < 1.2$  and  $p < 0.02$  according to ASTM E900-02 [41].
- In addition, the results obtained by applying this methodology verify the observation performed by Fisher et al., in which  $K_{IC}$  varies from about  $35 \text{ MPa} \cdot \sqrt{\text{m}}$  (at  $T = \Delta RT_{DBT} - 50 \text{ }^\circ\text{C}$ ) to about  $200 \text{ MPa} \cdot \sqrt{\text{m}}$  (at  $T = \Delta RT_{DBT} + 50 \text{ }^\circ\text{C}$ ).
- According to the methodology outputs, it would be recommended that the brittle fracture should be specially monitored under  $150 \text{ }^\circ\text{C}$ . This agrees with the conclusions of Pachur [67] that showed an irradiation temperature of  $150 \text{ }^\circ\text{C}$  produces the greatest

brittleness of the material, this being less for a higher temperature since irradiation temperature favors the repair of defects by annealing.

In summary, this analytical method allows to save time and reduce costs related to trial-and-error tests to make a decision on the suitability and safety of different candidate materials. The new formulation of the brittle fracture mathematical criterion helps make a decision from the analysis of standardized requirements (discrete variables) using a multicriteria approach solved as a decision matrix (risk matrix). In addition, the chemical composition restrictions obtained by the analytical model can be useful to be incorporated in technical guides for materials inspection.

In the future, this methodology could be used to predict the suitability of materials for other demanding applications, being a useful tool for materials selection tasks considering a design-for-reliability approach.

**Author Contributions:** Conceptualization, A.R.-P.; Formal analysis, A.R.-P.; Funding acquisition, A.R.-P. and A.M.C.; Investigation, A.R.-P., M.C., E.P. and G.L.; Methodology, A.R.-P. and A.M.C.; Project administration, A.R.-P. and A.M.C.; Resources, A.R.-P., M.C. and A.M.C.; Supervision, A.R.-P.; Validation, A.R.-P.; Writing—original draft, A.R.-P.; Writing—review and editing, A.R.-P., M.C., E.P., G.L. and A.M.C. All authors have read and agreed to the published version of the manuscript.

**Funding:** This work is part of the scope of activities included in the transfer contract of research results with reference 2019-CTINV-0068. This work has been funded by the project 2021V/-TAJOV/006 from the UNED Call for Research Projects named “Young Talents 2021” and by the Annual Grants Call of the E.T.S.I. Industriales of UNED through the project of reference 2022-ETSII-UNED-01.

**Institutional Review Board Statement:** Not applicable.

**Informed Consent Statement:** Not applicable.

**Data Availability Statement:** Not applicable.

**Acknowledgments:** This work has been realized in the framework of the activities of the Research Group of the UNED “Industrial Production and Manufacturing Engineering (IPME)” and the Industrial Research Group “Advanced Failure Prognosis for Engineering Applications”.

**Conflicts of Interest:** The authors declare no conflict of interest.

## Abbreviations

$\Delta RT_{DBT}$	Ductile-to-brittle transition temperature shift
API	American Petroleum Institute
ASME	American Society of Mechanical Engineers
BCC	Body-Centered Cubic
CRP	Copper-Rich Precipitates
FAD	Failure Assessment Diagrams
FCC	Face-Centered Cubic
FFS	Fitness For Service
HCP	Hexagonal Close-Packed
$K_I$	Stress concentration factor applied under normal conditions on the crack
$K_I$	Stress intensity factor
$K_{IC}$	Fracture toughness based on crack initiation determined at crack end temperature
$L_r$	Cutoff value
LWR	Light Water Reactor
NRC	U.S. Nuclear Regulatory Commission
RIL	Risk of integrity loss
RPV	Reactor pressure vessel
$RT_{DBT}$	Reference temperature
$RT_{DBT-I}$	Ductile-to-brittle transition temperature before irradiation
$RT_{DBT-NI}$	Ductile-to-brittle transition temperature after irradiation
SMD	Stable Matrix Defects
$\Phi$	Neutron flux

## References

1. IPCC. *Climate Change 2014: Synthesis Report. Contribution of Working Groups I, II and III to the Fifth Assessment Report of the Intergovernmental Panel on Climate Change*; Intergovernmental Panel on Climate Change (IPCC): Geneva, Switzerland, 2014.
2. Wang, C.-N.; Dang, T.-T.; Tibo, H.; Duong, D.-H. Assessing renewable energy production capabilities using DEA window and Fuzzy TOPSIS model. *Symmetry* **2021**, *13*, 334. [[CrossRef](#)]
3. Slugeň, V.; Sojak, S.; Egger, W.; Krsjak, V.; Simeg Veternikova, J.; Petriska, M. Radiation damage of reactor pressure vessel steels studied by positron annihilation spectroscopy—A Review. *Metals* **2020**, *10*, 1378. [[CrossRef](#)]
4. Murty, K.L.; Seok, C.S. Fracture in ferritic reactor steel—Dynamic strain aging and cyclic loading. *JOM* **2001**, *53*, 23–26. [[CrossRef](#)]
5. Oh, E.; Lee, H. An imbalanced data handling framework for industrial big data using a gaussian process regression-based generative adversarial network. *Symmetry* **2020**, *12*, 669. [[CrossRef](#)]
6. Faizi, S.; Salabun, W.; Ullah, S.; Rashid, T.; Więckowski, J. A new method to support decision-making in an uncertain environment based on normalized interval-valued triangular fuzzy numbers and COMET technique. *Symmetry* **2020**, *12*, 516. [[CrossRef](#)]
7. Allan, V. *Manufacture of Pressure Vessels for light Water Reactor Core and the Pressure Vessels for Reactor Core*. China Patent CN1015948B, 16 October 1987.
8. Rodríguez-Prieto, A.; Frigione, M.; Kickhofel, J.; Camacho, A.M. Analysis of the technological evolution of materials requirements included in reactor pressure vessel manufacturing codes. *Sustainability* **2021**, *13*, 5498. [[CrossRef](#)]
9. Arroyo Martínez, B.; Álvarez Laso, J.A.; Gutiérrez-Solana, F.; Cayón Martínez, A.; Jirón Martínez, Y.J.; Seco Aparicio, A.R. A proposal for the application of failure assessment diagrams to subcritical hydrogen induced cracking propagation processes. *Metals* **2019**, *9*, 670. [[CrossRef](#)]
10. Ferroni, P. *LWR Pressure Vessel Embrittlement and Conditions of Validity of Current Predictive Methodologies*; Department of Nuclear Engineering, Massachusetts Institute of Technology (MIT) Publications: Boston, MA, USA, 2006.
11. Tanguy, B.; Bouchet, C.; Bugat, S.; Besson, J. Local approach to fracture based prediction of the  $\Delta RT_{56J}$  and  $\Delta RT_{KIC, 100}$  shifts due to irradiation for an A508 pressure vessel steel. *Eng. Fract. Mech.* **2006**, *73*, 191–206. [[CrossRef](#)]
12. Chou, H.W.; Huang, C.-C. Probabilistic structural integrity analysis of boiling water reactor pressure vessel under low temperature overpressure event. *Int. J. Nucl. Energy* **2015**, *2015*, 785041. [[CrossRef](#)]
13. Rodríguez-Prieto, A.; Camacho, A.M.; Aragón, A.M.; Sebastián, M.A.; Yanguas-Gil, A. Polymers selection for harsh environments to be processed using additive manufacturing techniques. *IEEE Access* **2018**, *6*, 29899–29911. [[CrossRef](#)]
14. Yankova, M.S.; Jivkov, A.P.; Patel, R. Incorporation of obstacle hardening into local approach to cleavage fracture to predict temperature effects in the ductile to brittle transition regime. *Materials* **2021**, *14*, 1224. [[CrossRef](#)] [[PubMed](#)]
15. Bai, X.; Wu, S.; Liaw, P.K.; Shao, L.; Gigax, J. Effect of heavy ion irradiation dosage on the hardness of SA508-IV reactor pressure vessel steel. *Metals* **2017**, *7*, 25. [[CrossRef](#)]
16. Smirnov, A.; Smirnova, E.; Alexandrov, S. A new experimental method for determining the thickness of thin surface layers of intensive plastic deformation using electron backscatter diffraction data. *Symmetry* **2020**, *12*, 677. [[CrossRef](#)]
17. Li, Q.; Shen, Y.; Zhu, J.; Huang, X.; Shang, Z. Evaluation of irradiation hardening of P92 steel under Ar ion irradiation. *Metals* **2018**, *8*, 94. [[CrossRef](#)]
18. Jitsukawa, S.; Suzuki, K.; Okubo, N.; Ando, M.; Shiba, K. Irradiation effects on reduced activation ferritic/martensitic steels—tensile, impact, fatigue properties and modelling. *Nucl. Fusion* **2009**, *49*, 733–737. [[CrossRef](#)]
19. Alamo, A.; Horsten, M.; Averty, X.; Materna-Morris, E.I.; Rieth, M.; Brachet, J.C. Mechanical behavior of reduced-activation and conventional martensitic steels after neutron irradiation in the range 250–450 degrees C. *J. Nucl. Mater.* **2000**, *283*, 353–357. [[CrossRef](#)]
20. Hojna, A. Overview of intergranular fracture of neutron irradiated austenitic stainless steels. *Metals* **2017**, *7*, 392. [[CrossRef](#)]
21. Li, M.; Sokolov, M.A.; Zinkle, S.J. Tensile and fracture toughness properties of neutron-irradiated CuCrZr. *J. Nucl. Mater.* **2009**, *393*, 36–46. [[CrossRef](#)]
22. Fabritsiev, S.A.; Pokrovsky, A.S. Effect of irradiation temperature on microstructure, radiation hardening and embrittlement of pure copper and copper-based alloy. *J. Nucl. Mater.* **2007**, *367*, 977–983. [[CrossRef](#)]
23. Sharma, G.; Mukherjee, P.; Chatterjee, A.; Gayathri, N.; Sarkar, A.; Chakravarty, J.K. Study of the effect of alpha irradiation on the microstructure and mechanical properties of nanocrystalline Ni. *Acta Mater.* **2013**, *61*, 3257–3266. [[CrossRef](#)]
24. Singh, B.N.; Horsewell, A.; Toft, P. Effects of neutron irradiation on microstructure and mechanical properties of pure iron. *J. Nucl. Mater.* **1999**, *271*, 97–101. [[CrossRef](#)]
25. Zinkle, S.J.; Singh, B.N. Microstructure of neutron-irradiated iron before and after tensile deformation. *J. Nucl. Mater.* **2006**, *351*, 269–284. [[CrossRef](#)]
26. Fukuda, M.; Hasegawa, A.; Tanno, T.; Nogami, S.; Kurishita, H. Property change of advanced tungsten alloys due to neutron irradiation. *J. Nucl. Mater.* **2013**, *442*, 273–276. [[CrossRef](#)]
27. Cockeram, B.V.; Smith, R.W.; Leonard, K.J.; Byun, T.S.; Snead, L.L. Development of microstructure and irradiation hardening of Zircaloy during low dose neutron irradiation at nominally 358 degrees C. *J. Nucl. Mater.* **2011**, *418*, 46–61. [[CrossRef](#)]
28. Onimus, F.; Bechade, J.L.; Duguay, C.; Gilbon, D.; Pilvin, P. Investigation of neutron radiation effects on the mechanical behavior of recrystallized zirconium alloys. *J. Nucl. Mater.* **2006**, *358*, 176–189. [[CrossRef](#)]
29. Marmy, P.; Leguey, T. Impact of irradiation on the tensile and fatigue properties of two titanium alloys. *J. Nucl. Mater.* **2001**, *296*, 155–164. [[CrossRef](#)]

30. Li, M.; Byun, T.S.; Snead, L.L.; Zinkle, S.J. Low-temperature thermally-activated deformation and irradiation softening in neutron-irradiated molybdenum. *J. Nucl. Mater.* **2008**, *377*, 409–414. [[CrossRef](#)]
31. Xiao, X. Fundamental mechanisms for irradiation-hardening and embrittlement: A review. *Metals* **2019**, *9*, 113. [[CrossRef](#)]
32. Cécile, M.; Christian, R.; Michel, S. *Symmetry and Physical Properties of Crystals*; Springer: Berlin/Heidelberg, Germany, 2014.
33. Odette, G.R.; Lucas, G.; Klingensmith, R. The influence of metallurgical variables on the temperature dependence of irradiation hardening in pressure vessel steels. In Proceedings of the 17th International Symposium on Effects of Radiation on Materials, Sun Valley, ID, USA, 20–23 June 1996; American Society for Testing and Materials: West Conshohocken, PA, USA; pp. 606–622.
34. Ghoniem, N.M.; Kioussis, N. *Multiscale Modeling of the Deformation of Advanced Ferritic Steels for Generation IV Nuclear Energy*; Report DE-FC07-06ID14748; International Nuclear Energy Research Initiative (I-NERI): Washington, DC, USA, 2009.
35. Zhang, Y.; Gao, Y.; Sun, C.; Schwem, D.; Jiang, C.; Gan, J. Symmetry breaking during defect self-organization under irradiation. *Mater. Theory* **2020**, *4*, 4. [[CrossRef](#)]
36. Fukuya, K. Current understanding of radiation-induced degradation in light water reactor structural materials. *J. Nucl. Sci. Technol.* **2013**, *50*, 213–254. [[CrossRef](#)]
37. Torronen, K.; Pelli, R.; Planman, T.; Valo, M. *Irradiation Embrittlement Mitigation (NEA-CSNI-R-94-1)*; Nuclear Energy Agency of the OECD (NEA): Paris, France, 1993.
38. *ASME Boiler & Pressure Vessel Code (BPVC)*; American Society of Mechanical Engineers: New York, NY, USA, 2019.
39. Rodríguez-Prieto, A.; Primera, E.; Callejas, M.; Camacho, A.M. Reliability-based evaluation of the suitability of polymers for additive manufacturing intended to extreme operating conditions. *Polymers* **2020**, *12*, 2327. [[CrossRef](#)] [[PubMed](#)]
40. Eason, E.D.; Wright, J.E.; Odette, G.R. *Improved Embrittlement Correlations for Reactor Pressure Vessel Steels*; NUREG/CR-6551; U.S. Nuclear Regulatory Commission (NRC): Washington, DC, USA, 1998.
41. *ASTM E900*; Standard Guide for Predicting Radiation-Induced Transition Temperature Shift in Reactor Vessel Materials. American Society for Testing and Materials: Philadelphia, PA, USA, 2002.
42. Lie, S.T.; Yang, Z.M. BS7910:2005 Failure assessment diagram (FAD) on cracked circular hollow section (CHS) welded joints. *Adv. Steel Constr.* **2009**, *5*, 406–420.
43. Nissan, E. An Overview of AI Methods for in-Core Fuel Management: Tools for the Automatic Design of Nuclear Reactor Core Configurations for Fuel Reload, (Re)arranging New and Partly Spent Fuel. *Designs* **2019**, *3*, 37. [[CrossRef](#)]
44. Montassir, S.; Yakoubi, K.; Moustabchir, H.; Elkhalfi, A.; Rajak, D.K.; Pruncu, C.I. Analysis of crack behaviour in pipeline system using FAD diagram based on numerical simulation under XFEM. *Appl. Sci.* **2020**, *10*, 6129. [[CrossRef](#)]
45. Petrović, D.V.; Tanasijević, M.; Stojadinović, S.; Ivaz, J.; Stojković, P. Fuzzy model for risk assessment of machinery failures. *Symmetry* **2020**, *12*, 525. [[CrossRef](#)]
46. Rodríguez-Prieto, A.; Camacho, A.M.; Mendoza, C.; Lomonaco, G. Evolution of standardized specifications on materials, manufacturing and in-service inspection of nuclear reactor vessels. *Sustainability* **2021**, *13*, 10510. [[CrossRef](#)]
47. Smith, C.; Nanstad, R.; Odette, R.; Clayton, D.; Matlack, K.; Ramuhalli, P.; Light, G. *Roadmap for Nondestructive Evaluation of Reactor Pressure Vessel Research and Development by the Light Water Reactor Sustainability Program*; ORNL/TM-2012/380; International Atomic Energy Agency (IAEA): Vienna, Austria, 2012; p. 56.
48. *IAEA-145*; Non-Destructive Testing for Reactor Core Components and Pressure Vessels. International Atomic Energy Agency (IAEA): Vienna, Austria, 1971; p. 537.
49. Rodríguez-Prieto, A. *Análisis de Requisitos Tecnológicos de Materiales Especificados en Normativas Reguladas y su Repercusión Sobre la Fabricación de Recipientes Especiales para la Industria Nuclear*. Ph.D. Thesis, Universidad Nacional de Educación a Distancia, Madrid, Spain, 2014; p. 457.
50. Steele, L.E. *Neutron Irradiation Embrittlement of Reactor Pressure Vessel Steels*; International Atomic Energy Agency Publications: Vienna, Austria, 1975.
51. Yoon, K.K. *Fracture Toughness Data Analysis Using the Master Curve Method*; WRC Bulletin No. 486 Part 3; Welding Research Council (WRC): Shaker Heights, OH, USA, 2003.
52. *API 579-1/ASME FFS-1. Fitness-for-Service*, 2nd ed.; American Petroleum Institute (API): Washington, DC, USA, 2016.
53. *R.G 1.99 Rev.2*; Radiation Embrittlement of Reactor Vessel Materials. Nuclear Regulatory Commission (NRC): Washington, DC, USA, 1988; pp. 1–9.
54. Kirk, M.; Santos, C.; Eason, E.; Wright, J.; Odette, G.R. Updated embrittlement trend curve for reactor pressure vessel steels. In Proceedings of the 17th International Conference on Structural Mechanics in Reactor Technology (SMiRT 17), Prague, Czech Republic, 17–22 August 2003.
55. Rodríguez-Prieto, A.; Camacho, A.M.; Sebastián, M.A. Selection of candidate materials for reactor pressure vessels using irradiation embrittlement prediction models and a stringency level methodology. *Proc. Inst. Mech. Eng. Part L* **2019**, *233*, 965–976.
56. Amayev, A.D.; Kryukov, A.M.; Sokolov, M.A. Recovery of the transition temperature of irradiated WWER-440 Vessel Metal by Annealing. In *Radiation Embrittlement of Nuclear Reactor Pressure Vessels Steels: An International Review*; Steele, L.E., Ed.; American Society for Testing and Materials: Philadelphia, PA, USA, 1993; p. 374.
57. Server, W.L.; Lott, R.G.; Rosinski, S.T.; English, C. Recent surveillance data and a revised embrittlement correlation. *J. ASTM Int.* **2005**, *2*, 1–10. [[CrossRef](#)]
58. Ritchie, R.O.; Thompson, A.W. On macroscopic and microscopic analyses for crack initiation and crack growth toughness in ductile alloys. *Metall. Trans. A* **1985**, *16A*, 233–248. [[CrossRef](#)]

59. ASME B&PVC XI; Rules for In-Service Inspection of Nuclear Power Plant Components, Division 1, Rules for Inspection and Testing of Components of Light-Water-Cooled Plants. American Society of Mechanical Engineers (ASME): New York, NY, USA, 2021; pp. 1–784.
60. ASME B&PVC VIII; Rules for Construction of Pressure Vessels, Division 1. American Society of Mechanical Engineers (ASME): New York, NY, USA, 2021; pp. 1–804.
61. KTA 3201.2; Components of the Reactor Coolant Pressure Boundary of Light Water Reactors Part 2: Design and Analysis. Nuclear Safety Standards Commission (KTA): Salzgitter, Germany, 2017; pp. 1–162.
62. Cicero, S.; Fuentes, J.D.; Procopio, I.; Madrazo, V.; González, P. Critical distance default values for structural steels and a simple formulation to estimate the apparent fracture toughness in U-Notched conditions. *Metals* **2018**, *8*, 871. [[CrossRef](#)]
63. BS 7910; Guide on Methods for Assessing the Acceptability of Flaws in Fusion Welded Structures. British Standard Institution: London, UK, 2019.
64. Kim, Y.K.; Oh, B.T.; Kim, J.H. Effects of crack tip constraint on the fracture toughness assessment of 9% Ni steel for cryogenic application in liquefied natural gas storage tanks. *Materials* **2020**, *13*, 5250. [[CrossRef](#)] [[PubMed](#)]
65. Matvienko, Y.G. Failure Assessment Diagrams in Structural Integrity Analysis. In *Damage and Fracture Mechanics*; Boukharouba, T., Elboujdaini, M., Pluinage, G., Eds.; Springer: Dordrecht, The Netherlands, 2009; pp. 173–182.
66. Vaze, K.K. Structural integrity aspects of reactor safety. *Sadhana Acad. Proc. Eng. Sci.* **2013**, *38*, 971–997. [[CrossRef](#)]
67. Pachur, D. Apparent embrittlement saturation and radiation mechanisms of reactor pressure vessel steels. *ASTM STP* **1981**, *725*, 5–19.
68. Rodríguez-Prieto, A.; Camacho, A.M.; Sebastián, M.A. Materials selection criteria for nuclear power applications: A decision algorithm. *JOM* **2016**, *68*, 496–506. [[CrossRef](#)]
69. Rodríguez-Prieto, A.; Camacho, A.M.; Sebastián, M.A. Multicriteria materials selection for extreme operating conditions based on a multiobjective analysis of irradiation embrittlement and hot cracking prediction models. *Int. J. Mech. Mater. Des.* **2018**, *14*, 617–634. [[CrossRef](#)]
70. Fisher, S.B.; Harbottle, J.E.; Aldridge, N. Radiation hardening in magnox pressure-vessel steels. *Philos. Trans. A. Math. Phys. Eng. Sci.* **1985**, *315*, 301–332.
71. KTA 3203; Monitoring the Radiation Embrittlement of Material of the Reactor Pressure Vessel of Light Water Reactors. Nuclear Safety Standards Commission (KTA): Salzgitter, Germany, 2017; pp. 1–18.
72. ASME B&PVC III; Rules for Construction of Nuclear Facility Components-Division 1-Subsection NE-Class MC Components. American Society of Mechanical Engineers (ASME): New York, NY, USA, 2021; pp. 1–176.